American Mineralogist, Volume 93, pages 831–843, 2008

Effect of chemical environment on the hydrogen-related defect chemistry in wadsleyite

YU NISHIHARA,[1,2,3,*] TORU SHINMEI,[1,4] AND SHUN-ICHIRO KARATO[1]

[1]Department of Geology and Geophysics, Yale University, New Haven, Connecticut 06520, U.S.A.
[2]Department of Earth and Planetary Sciences, Tokyo Institute of Technology, Tokyo 152-8551, Japan
[3]Research Center for the Evolving Earth and Planets, Tokyo Institute of Technology, Tokyo 152-8551, Japan
[4]Geodynamics Research Center, Ehime University, Matsuyama 790-8577, Japan

ABSTRACT

The effect of chemical environment on the hydrogen-related defect chemistry in wadsleyite was investigated using Fourier-transform infrared (FTIR) spectroscopy. Samples were annealed at P = 14–16 GPa and T = 1230–1973 K using Kawai-type multi-anvil apparatus. The effect of oxygen fugacity (f_{O_2}) was investigated using three metal-oxide buffers (Mo-MoO_2, Ni-NiO, and Re-ReO_2). The effect of water fugacity (f_{H_2O}) was studied using two different capsule assemblies ("nominally dry" and "dry" assemblies). A range of total OH concentration ($C_{OH,Total}$) of studied wadslyeites varies between <50 H/10^6Si (<3 wt ppm H_2O) and 23 000 H/10^6Si (1400 wt ppm H_2O). The observed FTIR spectra were classified into four different classes, i.e., peaks at 3620 ("3620"), 3480 ("3480"), and 3205 cm^{-1} ("3205") and the others (Group O), where the Group O includes peaks at 3270, 3330, and 3580 cm^{-1}. The variation in OH concentration corresponding to each peak was analyzed separately. The OH concentrations correspond to "3620," "3480," and "3205" were found to be highly dependent on both f_{H_2O} and f_{O_2}. Assuming $C_{OH,Group\ O} = 2[(2H)_M^x]$ ($C_{OH,Group\ O}$ is OH concentration of Group O), present data were analyzed by using thermodynamic model for concentration of hydrogen-related defects. Based on analytical results, OH concentration of "3620" and "3480" was found to be reasonably explained by q = 1/2 and r = 1/12 (q and r are f_{H_2O} and f_{O_2} exponents, respectively), whereas that of "3205" was consistent with q = 1/2 and r = –1/12. These results suggest that "3620" and "3480" correspond to $H_M^{'}$ whereas "3205" corresponds to $H^{\bullet}$, respectively, under the charge neutrality condition of $[Fe_M^{'}] = 2[V_M^{''}]$.

Keywords: Wadsleyite, water, hydrogen-related defect, oxygen fugacity, mantle transition zone

INTRODUCTION

Wadsleyite [β-$(MgFe)_2SiO_4$] is considered as a potential host of water in the Earth's mantle transition zone (e.g., Smyth 1987; Inoue et al. 1995; Kohlstedt et al. 1996). Recently, water content in the mantle transition zone has been estimated by a combination of geophysical observations, such as electrical conductivity and seismic velocity, and physical properties of constituent minerals (e.g., Blum and Shen 2004; Huang et al. 2005; Hae et al. 2006; Ichiki et al. 2006). Although the estimates of water content by these studies vary from ~0.005 to ~0.5 wt% H_2O (much smaller than the solubility limit in wadsleyite, ~3 wt%), these amounts of water are considered to play an important role in transport properties in the mantle transition zone. Therefore, it is important to understand nature of hydrogen-related defects in wadsleyite.

There are several studies on hydrogen in wadsleyite. The significant solubility of water in wadsleyite was first predicted theoretically by Smyth (1987), and the solubility of ~3 wt% H_2O was later confirmed experimentally (e.g., Inoue et al. 1995; Kohlstedt et al. 1996). The effects of temperature and pressure on water solubility were studied by Demouchy et al. (2005). The location of hydrogen atom in wadsleyite lattice has been investigated based on FTIR spectroscopy, single-crystal X-ray diffraction and NMR (Kudoh and Inoue 1999; Kohn et al. 2002; Jacobsen et al. 2005). However, there is no systematic study on the effect of chemical environments, such as oxygen fugacity (f_{O_2}) and water fugacity (f_{H_2O}), on hydrogen-related defects in wadsleyite. The previous studies have focused on the incorporation mechanism of the majority of hydrogen in wadsleyite. It is well understood from crystal chemistry and experimental observation of a good correlation between Mg/Si ratio and the water content (e.g., Smyth 1987; Inoue et al. 1995). Two hydrogen atoms are incorporated into the crystal lattice coupled with an M-site vacancy, which yields a neutral (no effective electric charge) point defect, $(2H)_M^x$. In contrast, the nature of minor hydrogen-related defects in wadsleyite other than $(2H)_M^x$ is not well known due to their lower concentration. However, the minor charged defects may play more important roles in transport properties, such as rheological properties and electrical conductivity (Karato 2006). Since the concentration of defect is a function of many parameters characterizing chemical environments (e.g., f_{O_2}, f_{H_2O}, oxide activity), the effect of chemical environments on point defect chemistry provides a useful insight into the atomistic mechanisms of hydrogen dissolution and the way in which hydrogen affects

* E-mail: yuu@geo.titech.ac.jp

physical properties. Thus, a systematic study on the hydrogen-related defects in wadsleyite with special emphasis on the effect of chemical environments is needed.

In this study, we have investigated the effect of chemical environment on hydrogen-related defects in $(Mg,Fe)_2SiO_4$ wadsleyite using Fourier-transform infrared (FTIR) spectroscopy. In the previous study, we have investigated grain-growth kinetics of wadsleyite under wide range of water content, f_{O_2} and temperature (Nishihara et al. 2006a). Samples described by Nishihara et al. (2006a) were used in this study with some additional samples. The samples were annealed at P = 14–16 GPa and T = 1230–1973 K using a Kawai-type multi-anvil apparatus. The effect of f_{O_2} was investigated using three metal-oxide buffers. The effect of f_{H_2O} (water content) was studied using two different capsule assemblies. We were able to synthesize very dry wadsleyite (<50 H/10^{6}Si) using a newly developed "dry" sample assembly. This allowed us to investigate the influence of chemical environment on the hydrogen-related defects in a wide range of chemical environments.

Experimental methods

Generation of high-pressure and high-temperature and control of chemical environment

High-pressure and high-temperature annealing experiments were carried out with a KIWI 1000-ton Kawai-type multi-anvil apparatus installed at Yale University. We used an octahedral Cr_2O_3-doped MgO pressure medium with 14 mm edge length with 7 or 8 mm truncation edge length of WC anvils. To reduce the temperature gradient, a stepped $LaCrO_3$ heater was used and inserted in a ZrO_2 thermal insulation sleeve. Temperature is monitored using a W5Re-W26Re thermocouple. In all runs, all the ceramic components of the sample assembly were dried at 1200 K prior to high-pressure experiments for at least 2 h to remove adsorbed water.

To determine the effects of f_{O_2} on hydrogen-related defect chemistry in wadsleyite, we controlled f_{O_2} using three different metal-oxide buffers (Mo-MoO_2, Ni-NiO, and Re-ReO_2). The control of f_{O_2} by solid-state buffers in a multi-anvil apparatus has been well established (e.g., Rubie et al. 1993). The oxygen fugacities for the metal-oxide buffers at the studied pressure and temperature conditions are calculated based on ambient pressure data for the buffers (O'Neill 1986; O'Neill and Pownceby 1993; Pownceby and O'Neill 1994) with the correction for the pressure effect using the molar volumes of relevant materials (Robie et al. 1978). More detailed description on the calculation of f_{O_2} is given in Nishihara et al. (2006a). The presence of oxide (MoO_2, NiO, and ReO_2) was checked by SEM observations and micro-Raman analyses after the annealing experiments but was not observed. Although grain-growth of wadsleyite is sensitive to the metallic capsule material, the grain-size after annealing is uniform (Nishihara et al. 2006a). We take this as an evidence for chemical equilibrium with respect to f_{O_2}. As described by Nishihara et al. (2006a), some samples that showed heterogeneous grain-size distribution after annealing experiments suggesting incomplete equilibrium with respect to the f_{O_2} within the capsule were not considered in this study.

To investigate the effects of f_{H_2O} (OH concentration) on hydrogen-related defect chemistry in wadsleyite, we have conducted experiments on samples with largely different OH concentrations: "dry" and "nominally dry" experiments (Table 1). The details of the sample assemblies and the methods for conducting experiments will be described in the following section.

Annealing experiments

Starting materials for the annealing experiments are sintered wadsleyite aggregates that were obtained by the transformation from San Carlos olivine powder at P = 14–15 GPa and T = 1230–1573 K. The only exceptions are runs K22 and K95, in which San Carlos olivine powder was used as starting material. Hydroxyl content of wadsleyite starting materials range from <50 to 20 000 H/10^{6}Si (<3 to 1200 wt ppm H_2O). For "dry" annealing experiments, relatively dry starting materials that were synthesized using a sealed 75% Au–25% Pd capsule were used. The water content of these samples are C_{OH} <50 H/10^{6}Si for Mo and Ni capsule experiments and 400 H/10^{6}Si for Re capsule experiments.

In "dry" annealing experiments, wadsleyite was enclosed in each metal foil capsule (Mo, Ni, or Re) and put in a 75% Au–25% Pd capsule of 1.6 mm outer diameter and 0.1 mm thick (see Fig. 2 of Nishihara et al. 2006a). Contamination of hydrogen was minimized by using this welded capsule. An Al_2O_3 sleeve is inserted between a metal foil and an AuPd capsule to avoid reaction between the metal foil and an AuPd capsule. In "nominally dry" runs, a wadsleyite sample was surrounded by a fine-grained San Carlos olivine powder to protect the sample from shock during initial stage of compression and put in the central part of each metal capsule made up of two layers of 25 μm thick foil. In these experiments, no hydrous mineral was used, but the capsule was not welded shut, consequently, some amount of hydrogen was incorporated into the sample from surrounding ceramic parts or cement.

For all experiments, the capsule containing the sample was vacuum-dried at ~400 K for more than 10 h prior to mechanical sealing by crimping or welding. The length of the capsules after packing was ~2.7 mm. Pressure and temperature conditions of the annealing experiments are at P = 14–16 GPa and T = 1230–1973 K. Recovered samples were examined using a Raman spectrometer for phase identification, and optical microscope and an SEM for microstructural observation. The grain-growth kinetics of wadsleyite was studied using same run products and is reported by Nishihara et al. (2006a).

Fourier-transform infrared spectroscopy (FTIR)

In this experimental study, we analyzed aggregate samples, therefore only orientationally averaged data can be obtained. However, some IR absorbers in wadsleyite are highly anisotropic (Jacobsen et al. 2005). Thus, to derive representative (well-averaged) FTIR pattern from the aggregate, we selected samples in which more than 300 grains are included in total analyzed area. For some samples from Nishihara et al. (2006a), only small number of grains (<300 grains) are included in total analyzed area due to large grain-size compared to total sample size. These data were not used in this study.

The OH concentrations in the annealed sample were measured using a Fourier-transform infrared (FTIR) spectrometer, Digilab Excalibur 3000, attached with UMA-500 FTIR microscope. Measurements were carried out using mid-IR light, a KBr beam splitter and an MCT detector. Non-polarized IR beam with dimension of 40 × 40 μm was used. For FTIR measurements, samples were doubly polished to a thickness of 50–200 μm. Samples were directly put on a KBr mount disk. The grain-size of wadsleyite was from 1.1 μm (K133Ni and K133Re) to 10.8 μm (K136Re). Generally, 2–7 measurements were carried out for each sample, and averaged hydroxyl content was adopted in the subsequent analyses. Consequently, under these analytical conditions, total analyzed volume for each sample includes >300 grains. The IR spectra were obtained by more than two hundred scans with 4 cm^{-1} resolution. Background corrections of absorbance spectra were performed by a spline fit of the baseline. The concentrations of hydroxyl were calculated using the calibration by Paterson (1982) as follows:

$$C_{OH} = \frac{B}{150\zeta}\int \frac{H(\nu)}{3780-\nu}d\nu \quad (1)$$

where C_{OH} is the molar concentration of hydroxyl, ζ is an orientation factor, and $H(\nu)$ is the absorption coefficient in cm^{-1} at wavenumber ν in cm^{-1}. The value of B = 4.08 × 10^4 H/10^{6}Si was used for $(Mg_{0.9}Fe_{0.1})_2SiO_4$ wadsleyite based on published data of density (Kohlstedt et al. 1996). Assuming random orientation, a value of ζ = 1/3 was used for sintered polycrystalline wadsleyite analyzed in present study (Kohlstedt et al. 1996). In this study, we primarily use H/10^{6}Si for unit of hydrogen concentration (C_{OH}). For $(Mg_{0.9}Fe_{0.1})_2SiO_4$ wadsleyite, the relationship between values of C_{OH} (H/10^{6}Si), C_{H_2O} (wt% H_2O) and C_{H_2O} (wt ppm H_2O) can be approximated as follows; C_{OH} (H/10^{6}Si) = 16 × 10^4 × C_{H_2O} (wt% H_2O) = 16 × C_{H_2O} (wt ppm H_2O). Libowitzky and Rossman (1996) argued that absorbance measurements using non-polarized IR beam yield quantitatively erroneous results due to the breakdown of linear relationship between absorbance and sample thickness. Thus we have examined and confirmed the linear relationship between absorbance and sample thickness for wadsleyite aggregates by the measurements of a sample with different thickness. The details of the testing measurements are described in Appendix 1.

Results

Recovered wadsleyite samples showed equigranular texture with no secondary phases at the level of scanning electron microscope observations (a resolution of ~0.1 μm). An FE-SEM image showing the microstructure of K133Ni is presented as Figure 1.

TABLE 1. Experimental conditions and results

Run no.	Capsule assembly	T (K)	P (GPa)	t (h)	$\log_{10} f_{O_2}$ (Pa)	N*	Total C_{OH} (H/10^{6}Si)	C_{OH} for individual IR peaks (H/10^{6}Si) "3620"	"3480"	"3205"	Group O
Mo capsule											
K88	Nom. dry	1450†	14.7	4	–1.83	3	23 000 +2000 –2000	1900 +200 –200	100 +150 –60	–	21 000 +2000 –2000
K53	Nom. dry	1670†	14.4	2	–0.15	3	9500 +1200 –1000	930 +170 –140	170 +90 –60	120 +60 –40	8300 +900 –800
K43	Nom. dry	1670†	14.4	4	–0.15	3	2300 +700 –500	130 +50 –30	40 +30 –20	190 +40 –30	1900 +800 –500
K48	Nom. dry	1890†	15.2	8	1.44	4	280 +80 –60	–	–	110 +10 –10	160 +90 –60
K45	Nom. dry	1890†	15.0	1	1.39	7	140 +40 –30	–	–	90 +30 –20	50 +30 –20
K136Mo	Dry	1973	15.8	48	2.03	2	69 +2 –2	–	–	36 +6 –5	33 +9 –7
K133Mo	Dry	1773	15.8	24	0.96	2	<50	–	–	–	–
Ni capsule											
K85	Nom. dry	1450†	14.7	4	1.64	4	16 000 +3000 –2000	3000 +600 –500	400 +220 –140	–	12 000 +3000 –2000
K50	Nom. dry	1670†	14.4	4	3.15	4	1900 +400 –300	420 +60 –60	90 +100 –50	50 +20 –10	1300 +500 –300
K65	Nom. dry	1890†	15.0	4	4.52	5	310 +140 –90	70 +50 –30	–	60 +20 –10	170 +130 –70
K136Ni	Dry	1973	15.8	48	5.08	2	73 +2 –2	–	–	31 +4 –3	42 +6 –5
K133Ni	Dry	1773	15.8	24	4.12	2	<50	–	–	–	–
Re capsule											
K22‡	Nom. dry	1230†	14.8	1	2.19	4	20 000 +2000 –1000	1500 +200 –200	210 +110 –70	–	19 000 +1000 –1000
K23	Nom. dry	1450†	14.5	4	3.92	4	4900 +800 –700	1200 +700 –400	510 +360 –210	–	3100 +200 –200
K136Re	Dry	1973	15.8	48	6.95	2	4200 +300 –300	1700 +300 –200	470 +70 –60	–	2000 +500 –400
K133Re	Dry	1773	15.8	24	6.16	2	680 +70 –70	330 +60 –50	50 +20 –20	–	280 +130 –90
K95‡	Dry	1670†	14.4	1	5.23	3	400 +120 –90	140 +20 –20	40 +60 –20	–	210 +80 –60

* Number of measurements per sample.
† Temperature was measured by thermocouple with Cu coil, and corrected to real temperature (Nishihara et al. 2006b).
‡ San Carlos olivine powder was used for starting material.

Total OH concentration in wadsleyite

Calculated total OH concentrations ($C_{OH,Total}$) of wadsleyites are listed in Table 1. In Figure 2, the total concentration of OH is plotted as a function of f_{O_2}. Total OH concentration in the recovered samples of "nominally dry" and "dry" experiments are $C_{OH,Total}$ = 140–23 000 H/10^{6}Si (9–1400 wt ppm H_2O) and <50–4200 H/10^{6}Si (<3–260 wt ppm H_2O), respectively. The OH concentration of "dry" samples annealed within Re capsule was relatively higher (up to 4200 H/10^{6}Si) than those within Mo and Ni capsules (typically <100 H/10^{6}Si). Although same calibration (after Paterson 1982) was used in this study and study by Nishihara et al. (2006a), presented values of total C_{OH} in the same sample are slightly different between these two studies. This is because C_{OH} was calculated directly from raw data in Nishihara

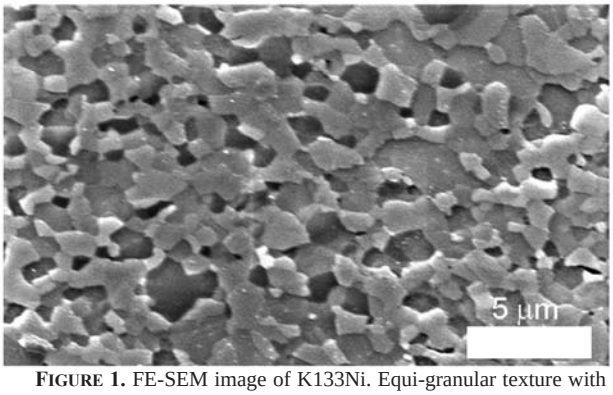

FIGURE 1. FE-SEM image of K133Ni. Equi-granular texture with no secondary phases was observed.

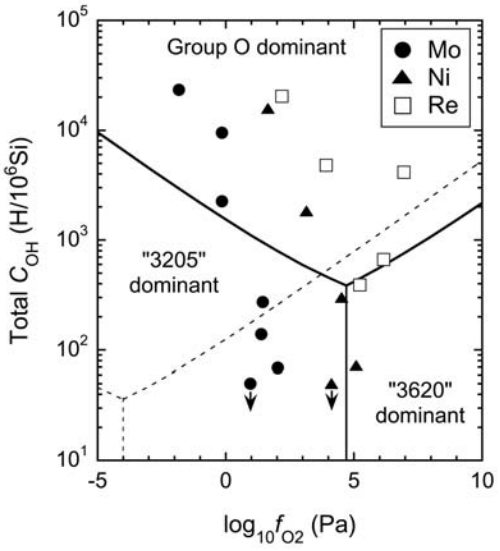

FIGURE 2. Plot of total OH concentration vs. oxygen fugacity. Solid circles, solid triangles, and open squares are experimental data collected using Mo, Ni, and Re capsules, respectively. Lines are boundaries of field of each dominant FTIR peak (or group) at T = 2100 K (thick solid lines) and 1600 K (thin broken lines). The boundaries are drawn based on the fitting of Equation 5 (using parameters with fixed q = 1/2 and r = 1/12 or –1/12, Table 2). Symbols with downward arrows indicate the upper limit of C_{OH}.

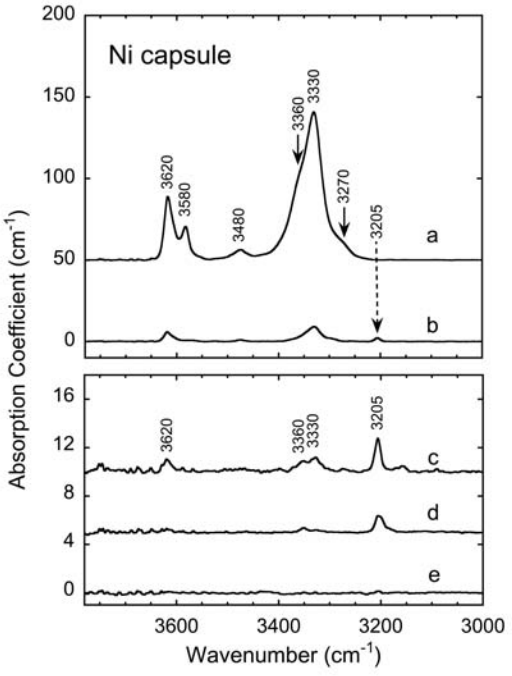

FIGURE 4. FTIR spectra of wadsleyite obtained from experiments with Ni capsule. Total hydroxyl contents are (**a**) $C_{OH,Total}$ = 16 000 H/10^{6}Si (run K85), (**b**) 1900 H/10^{6}Si (K50), (**c**) 310 H/10^{6}Si (K65), (**d**) 73 H/10^{6}Si (K136Ni), and (**e**) <50 H/10^{6}Si (K133Ni).

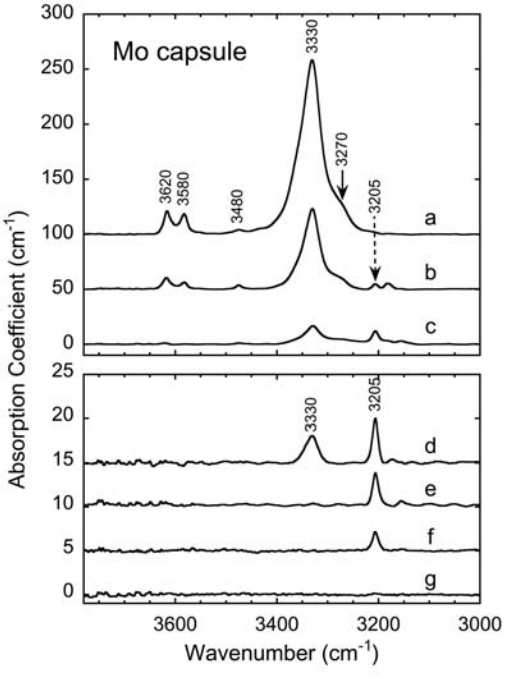

FIGURE 3. FTIR spectra of wadsleyite obtained from experiments with Mo capsule. Total hydroxyl contents are (**a**) $C_{OH,Total}$ = 23 000 H/10^{6}Si (run K88), (**b**) 9500 H/10^{6}Si (K53), (**c**) 2300 H/10^{6}Si (K43), (**d**) 280 H/10^{6}Si (K48), (**e**) 140 H/10^{6}Si (K45), (**f**) 69 H/10^{6}Si (K136Mo), and (**g**) <50 H/10^{6}Si (K133Mo).

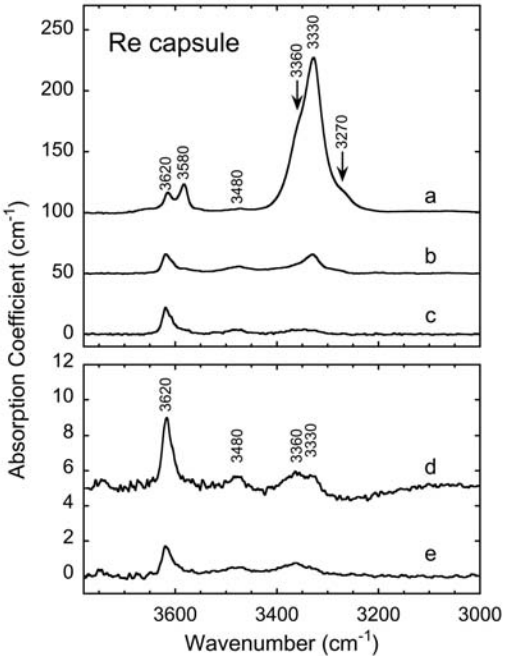

FIGURE 5. FTIR spectra of wadsleyite obtained from experiments with Re capsule. Total hydroxyl contents are (**a**) $C_{OH,Total}$ = 20 000 H/10^{6}Si (run K22), (**b**) 4900 H/10^{6}Si (K23), (**c**) 4200 H/10^{6}Si (K136Re), (**d**) 670 H/10^{6}Si (K133Re), and (**e**) 400 H/10^{6}Si (K95).

et al. (2006a) while C_{OH} was calculated based on Gaussian fit of data in this study (see below).

Characteristics of FTIR spectra of wadsleyite

Figures 3–5 show the spectra taken from experiments with Mo, Ni, and Re capsules, respectively. At OH concentration of $C_{OH,Total}$ ~20 000 H/10^{6}Si (Figs. 3a, 4a, and 5a), the spectra show the most intense absorption peak at 3330 cm^{-1}, modest peaks at 3580 and 3620 cm^{-1} and weaker peaks at 3270 and 3480 cm^{-1}. The FTIR spectra with $C_{OH,Total}$ ~20 000 H/10^{6}Si are consistent with those of previous studies with similar OH concentration (Kubo et al. 2004; Nishihara et al. 2006a).

In contrast, the FTIR spectra with a smaller amount of OH concentration ($C_{OH,Total}$ < ~10 000 H/10^{6}Si) show interesting features that are not previously reported: (1) the intensity ratio of absorption peaks strongly depends on the total OH concentration, and (2) the intensity ratios are different among the samples annealed in different capsules (Figs. 3–5).

In the FTIR spectra of wadsleyite annealed in a Mo capsule (Fig. 3), the peak at 3205 cm^{-1} is inconspicuous at $C_{OH,Total}$ = 23 000 H/10^{6}Si (Fig. 3a). However, with decreasing total OH concentration, this peak becomes increasingly more visible. Consequently, this peak is the only detectable peak in extremely hydrogen-poor samples ($C_{OH,Total}$ < 100 H/10^{6}Si, Figs. 3e and 3f).

In the case of wadsleyite annealed in a Re capsule, the IR spectra for $C_{OH,Total}$ = 20 000 H/10^{6}Si (Fig. 5a) are quite similar to those in a Mo capsule experiments at similar $C_{OH,Total}$ (Fig. 3a). However, in contrast to Mo capsule experiments, a peak at 3205 cm^{-1} does not appear with decreasing OH concentration in Re capsule experiments. Instead, a peak at 3620 cm^{-1}, which is present from higher OH concentration (Fig. 5a), survives at lower OH concentration (Figs. 5b–5d) although other peaks become very weak. Another feature of the spectra of samples annealed in a Re capsule is the behavior of the peak at 3480 cm^{-1}. The intensity of this peak decreases slowly with decreasing $C_{OH,Total}$ compared to a major peak at 3330 cm^{-1}. In previous studies using a single-crystal specimen (Kohn et al. 2002; Jacobsen et al. 2005), a band at ~3480 cm^{-1} is considered to consist of more than one peak. However, explicit splitting of this peak was not observed within a resolution of analysis in this study. Thus, we tentatively treat the peak at 3480 cm^{-1} as a single peak. A minute difference between Mo and Re capsule experiments can be also found at the higher wavenumber side of the large peak at 3330 cm^{-1}. A small shoulder peak at ~3360 cm^{-1} exists in the spectra of Re runs while no signature is found at same wavenumber in the spectra of Mo runs. The presence of this shoulder peak is more evident in the spectra with lower $C_{OH,Total}$ (Figs. 5d and 5e).

The behavior of IR spectra of samples annealed in a Ni capsule (Fig. 4) is intermediate to samples annealed in Mo and Re capsules. In samples annealed in a Ni capsule, both of 3620 and 3205 cm^{-1} peaks survive at relatively dry condition (Fig. 4c). The small shoulder peak at ~3360 cm^{-1} observed in Re capsule runs is also observed in the Ni runs.

Based on these observations we classify the FTIR absorption peaks in the OH vibration region into 4 classes. In each class, the variation of peak intensity with chemical environment is similar. The 4 classes are (1) a peak at 3620 cm^{-1} (hereafter "3620"); (2) a peak at 3480 cm^{-1} ("3480"); (3) a peak at 3205 cm^{-1} ("3205");

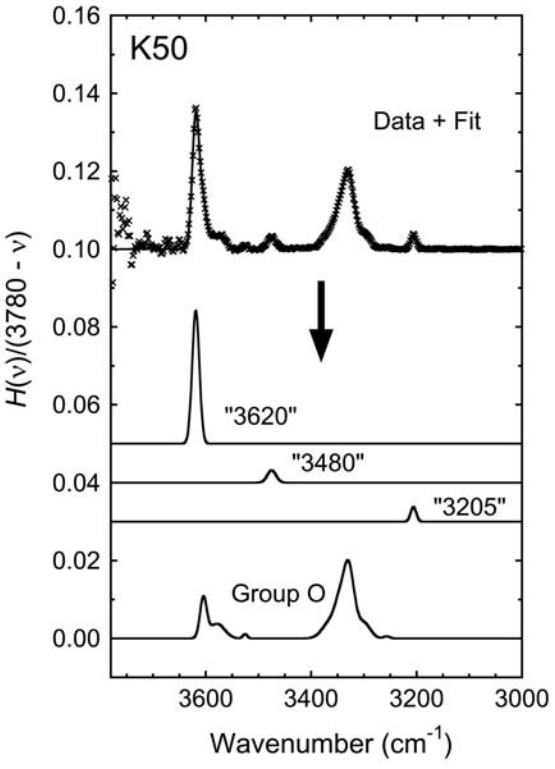

FIGURE 6. An example of deconvolution of FTIR pattern. Data (crosses in the top pattern) in $H(\nu)/(3780 - \nu)$ was fitted by Gaussian functions and was decomposed to peaks at 3620, 3480, and 3205 cm^{-1} ("3620," "3480," and "3205," respectively) and the other OH peaks (Group O).

and (4) the others (Group O). The Group O includes peaks at 3270, 3330, and 3580 cm^{-1}. A very small peak at ~3180 cm^{-1} observed in some samples is also included in the Group O. The small shoulder peak at ~3360 cm^{-1} is tentatively categorized into Group O since this peak is mostly unresolvable due to serious overlapping of the large neighboring peak at 3330 cm^{-1}. Thus, behavior of this peak is not discussed separately in the following sections. The deconvolution of FTIR spectra was made by fitting several Gaussian functions to the entire spectrum typically in the wavenumber range of 2950–3700 cm^{-1}. Considering the formula of Paterson (1982), we did not fit Gaussian functions directly to the absorption coefficient $H(\nu)$ (see Eq. 1). The Gaussian fits were made to the spectrum of $H(\nu)/(3780 - \nu)$. The peaks corresponding with Group O were also fitted with Gaussian as well as the three distinct peaks. Figure 6 shows an example of the pattern deconvolution. Calculated concentrations of the 4 classes of OH in all the analyzed samples are listed in Table 1.

For "3620," the wavenumber of fitted peak is at 3618–3621 cm^{-1} except for the two samples with the highest total C_{OH} (K22 and K88) for which the peak is at 3613 and 3615 cm^{-1}, respectively. A similar shift of peak position with increasing hydrogen concentration is reported by Jacobsen et al. (2005) (3619 cm^{-1} at $C_{OH,Total}$ = 2300 H/10^{6}Si and 3614 cm^{-1} at 50 000 and 15 000 H/10^{6}Si). The peak position of "3480" and "3205" is constant as a function of total C_{OH} and is in a range of 3478 ± 4 and 3205 ± 1 cm^{-1}, respectively.

DISCUSSION

Effect of chemical environment on concentration of hydrogen-related defects

As demonstrated above, peak intensity of various FTIR absorption peaks of wadsleyite does not change in the same way with chemical environment, and the capsule material and the total OH concentration affect the intensity of each peak in a different fashion. In the following section, we analyze data of OH concentration corresponding to individual peaks as a function of the chemical environments. The results of the analyses of experimental data will be compared with theoretical values of f_{O_2} and f_{H_2O} dependences. Based on the comparison, species of hydrogen-related defects and charge neutrality condition in wadsleyite will be discussed.

The concentration of a point defect in $(Mg,Fe)_2SiO_4$ minerals that are in chemical equilibrium with respect to a given chemical environment can be expressed by

$$[\mathrm{X}] \propto f_{H_2O}^{q} f_{O_2}^{r} a_{MO}^{s} \exp\left(-\frac{\Delta H_X(P)}{RT}\right) \quad (2)$$

where X is a type of defect, a_{MO} is the activity of an oxide MO (M is Mg or Fe), $\Delta H_X(P)$ is the formation enthalpy of defect X, R is the gas constant, and q, r, and s are the exponents for f_{H_2O}, f_{O_2}, and a_{MO}, respectively. The values of q, r, and s are specific to each defect and dependent, in general, on the charge neutrality conditions (those are in turn determined by the dominant charged species; see e.g., Karato 2008). When f_{H_2O}, f_{O_2}, and a_{MO} are buffered by a particular chemical reaction, they are functions of temperature and pressure [$f_{H_2O}(P,T)$, $f_{O_2}(P,T)$, and $a_{MO}(P,T)$].

The majority of hydrogen-related defects at high OH concentration are known to be two hydrogen atoms coupled with M-site vacancy, $(2H)_M^x$ (e.g., Smyth 1987; Inoue et al. 1995). Since $(2H)_M^x$ is a neutrally charged defect, q, r, and s for concentration of this defect are independent of charge neutrality condition. Concentration of this defect is expressed by

$$\left[\left(2\mathrm{H}\right)_M^{\times}\right] \propto f_{H_2O}^{1} f_{O_2}^{0} a_{MO}^{-1} \exp\left(-\frac{\Delta H_{(2H)_M^{\times}}(P)}{RT}\right) \quad (3)$$

(e.g., Karato 2008). Because Group O is the most abundant class at high OH concentration, Group O is considered to correspond to $(2H)_M^x$. If the oxide activity, a_{MO} is kept constant among the different runs, and the data at the same temperature and pressure are compared, the variation of peak intensity for Group O can be interpreted as due to the variation of f_{H_2O}. The influence of capsule material is most likely due to the influence of f_{O_2}. Consequently, our observations imply that some of the marked absorption peaks ("3620," "3480," and "3205") correspond to other hydrogen-related defects whose concentrations depend on f_{O_2} and f_{H_2O} differently from that of $(2H)_M^x$.

Since water fugacity f_{H_2O} was not directly controlled in this study, we could not directly apply Equation 2 for analysis of the present data. A measurable variable other than f_{H_2O} is necessary to express concentration of a defect, [X]. As described above, the majority of hydrogen-related defect in wadsleyite at high OH concentration is $(2H)_M^x$. Since we can assume $C_{OH,Group\ O} = 2[(2H)_M^x]$ ($C_{OH,Group\ O}$ is the concentration of Group O), using $C_{OH,Group\ O}$, a measurable parameter, the concentration of defect X can be expressed without f_{H_2O} by substituting Equation 2 for Equation 3 as

$$[\mathrm{X}] \propto (C_{OH,Group\ O})^{q} f_{O_2}^{r} a_{MO}^{q+s} \exp\left(-\frac{\Delta H_X(P) - q\Delta H_{(2H)_M^{\times}}(P)}{RT}\right) \quad (4)$$

Because pressure range in present data are relatively narrow (14–16 GPa), the activation enthalpy can be regarded as a constant. The a_{MO} was fixed in present experiments. Thus, Equation 4 can be reduced to

$$[\mathrm{X}] = A\,(C_{OH,Group\ O})^{q} f_{O_2}^{r} \exp\left(-\frac{\Delta H_X^*}{RT}\right) \quad (5)$$

where A is a constant and $\Delta H_x^* \equiv \Delta H_x - q\Delta H_{(2H)_M^x}$. In Equation 5, the effect of f_{H_2O} is expressed through the effect of $C_{OH,Group\ O}$. We have analyzed our data of [X] = $C_{OH,3620}$, $C_{OH,3480}$, and $C_{OH,3205}$ by fitting Equation 5, and derived A, q, r, and ΔH_X^* for "3620", "3480," and "3205".

Table 2 lists parameters derived by fitting Equation 5 to present data. In the present analysis, trade-off between parameters makes it difficult to determine all the parameters accurately. Figure 7 shows confidence ellipses in $q - r$ and $q - \Delta H_X^*$. As is clear from this figure, the values of r and ΔH_X^* correlate with q value, and real uncertainty is very large for these parameters. After discussion on defect chemistry in wadsleyite in the later section, we will adopt $q = 1/2$ and $r = 1/12$ for "3620" and "3480," and $q = 1/2$ and $r = -1/12$ for "3205." Table 2 also lists parameters derived by fits with fixed q and r values. First, we will discuss parameters derived from fits without any constraint (Table 2). For "3620" and "3480," the derived values of q, r, and ΔH_X^* are indistinguishable within the uncertainties (Table 2 and Fig. 7), and range from ~0.5 to ~1.2, ~0.05 to ~0.20, and from ~–50 to ~50 kJ/mol, respectively. For "3205," r has a negative value (–0.09 ± 0.05) that is in contrast to those for other "3620" and "3480." The ΔH_X^* for "3205" was determined to be 7 ± 107 kJ/mol (Table 2), which is similar to those for "3620" and "3480." However, as is clear from Figure 7, constraint for this parameter is very weak due to strong correlation with other parameters. All the derived parameters for "3620" and "3480" are indistinguishable suggesting that "3620" and "3480" correspond to the same type of hydrogen-related defect while "3205" corresponds to another type of defect.

Figures 8, 9, and 10 show OH concentrations of individual peaks as functions of $C_{OH,Group\ O}$, f_{O_2} and reciprocal temperature, respectively, at normalized conditions. Note that the normalization

TABLE 2. Parameters for Equation 5 for individual FTIR peaks

Parameter	"3620"		"3480"		"3205"	
$\log_{10} A$ (H/10^6Si)	–0.33 ± 0.56	–0.06 ± 0.65	–0.46 ± 0.72	0.28 ± 0.62	2.03 ± 2.51	5.36 ± 1.01
ΔH_X^* (kJ/mol)	16 ± 19	–28 ± 20	18 ± 22	3 ± 19	7 ± 107	158 ± 34
q	0.98 ± 0.14	[1/2]	0.82 ± 0.18	[1/2]	0.09 ± 0.26	[1/2]
r	0.13 ± 0.03	[1/12]	0.14 ± 0.04	[1/12]	–0.09 ± 0.05	[–1/12]

Note: Numbers in square brackets are fixed values in the parameter fitting.

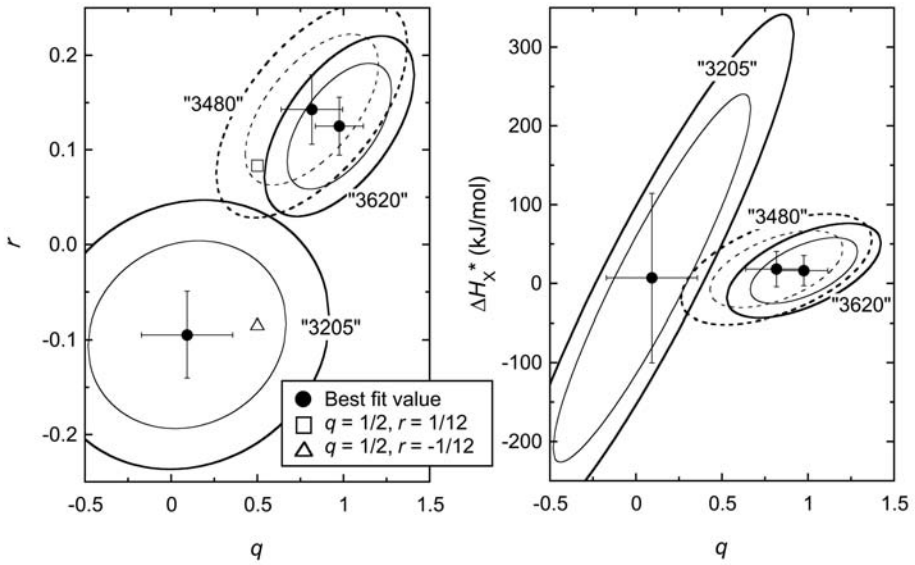

FIGURE 7. Confidence ellipses in $q - r$ (left) and $q - \Delta H_x^*$ (right) for fit of Equation 5. The inner thin ellipses and outer thick ellipses represent 1σ (68.3% confidence level) and 2σ (95.4% confidence level) limits, respectively. Solid circles are best fit values derived without constraints on q and r. Open squares and open triangles are q = 1/2 and r = 1/12, and q = 1/2 and r = –1/12, respectively. Parameters for "3620" and "3480" are indistinguishable within uncertainty. Our experimental results are reasonably explained by H_M' (q = 1/2 and r = 1/12) for "3620" and "3480" and by $H^{\bullet}$ (q = 1/2 and r = –1/12) for "3205" under the charge neutrality condition of $[Fe_M^{\bullet}] = 2[V_M'']$ (Table 4).

is carried out at constant value of $C_{OH,Group\ O}$, but not at constant f_{H_2O}. Thus the temperature dependence shown in Figure 10 is the relative temperature dependence of C_{OH} for individual peaks to $C_{OH,Group\ O}$. In Figures 8, 9, and 10, fitted parameters with fixed q = 1/2 and r = 1/12 or –1/12 (Table 2) were used to normalize experimental data in terms of f_{O_2}, T or $C_{OH,Group\ O}$, and the results of the fits are shown by solid lines. Similar plots for fit without any constraint on q and r are presented as on-line supplementary material (Supplementary Figs. 1–3)[1]. Lines in Figure 2 are calculated boundaries of the field of dominant FTIR peak (or group) at T = 2100 K (thick solid lines) and 1600 K (thin broken lines) based on parameters in Table 2.

Hydrogen-related defect chemistry in wadsleyite

To identify the types of defects corresponding to the marked FTIR peaks in wadsleyite, the experimental constraints on q and r were compared with theoretical values of exponents for concentration of hydrogen-related defects. The theoretical values of the exponents for chemical environments can be derived from the analysis of chemical reactions between defects (e.g., Stocker and Smyth 1978; Karato 2008). The concentration of charged defects is dependent on the effective charge neutrality condition in the crystal. However, the effective charge neutrality condition in wadsleyite is not well known. We offer the following three charge neutrality conditions as candidates for the dominant charge neutrality condition in wadsleyite.

TABLE 3. Exponents for concentration of neutral point defects

Defect	q	r	s
$[(2H)_M^{\times}]$	1	0	–1
$[(4H)_{Si}^{\times}]$	2	0	2
$[(HOH)_i^{\times}]$	1	0	0

Notes: Table shows dependence of concentrations of point defects in $(Mg,Fe)_2SiO_4$ minerals on chemical environment: $[X] \propto f_{H_2O}^q f_{O_2}^r a_{MO}^s$. These exponents for neutral defects are independent of charge neutrality condition.

It is known that Fe_3O_4 (magnetite) component dissolves into Fe_2SiO_4 spinel (ringwoodite) solid solution significantly at high pressure (P > 9 GPa) by forming $Fe_M^{\bullet}$ and Fe_{Si}' (and minor $Si_M^{\bullet\bullet}$) defects (Yamanaka et al. 1998; Koch et al. 2004). [The Kröger and Vink (1956) notation of point defect is used.] These defects are likely to exist in wadsleyite because the crystal structure of wadsleyite is closely related to that of the spinel structure (Horiuchi et al. 1982). Thus $[Fe_M^{\bullet}] = [Fe_{Si}']$ (K in Table A2) is one of the most probable charge neutrality conditions in wadsleyite. For chemical environment of typical mantle (in terms of f_{O_2} and oxide activity), charge neutrality in olivine is maintained by $[Fe_M^{\bullet}] = 2[V_M'']$ (F) at "dry" condition and $[Fe_M^{\bullet}] = [H_M']$ (A) at "wet" condition. Since olivine has the same stoichiometry $[(Mg,Fe)_2SiO_4]$ as wadsleyite, these two are also likely charge neutrality conditions. All three of these candidate charge neutrality conditions include ferric iron as the dominant charged defect. Incorporation of large amounts of ferric iron in wadsleyite is demonstrated by the results of Mössbauer spectroscopy on hydrous wadsleyite (McCammon et al. 2004).

Theoretically derived exponents of concentration for neutral hydrogen-related defects and charged ones under the three charge neutrality conditions are listed in Tables 3 and 4, respectively. Complete data of exponents of the defect concentration (including those for hydrogen-unrelated defects) at the three charge neutrality conditions are provided as on-line supplementary

[1] Deposit item AM-08-027, Supplementary Table 1 and Supplementary Figures 1–3. Deposit items are available two ways: For a paper copy contact the Business Office of the Mineralogical Society of America (see inside front cover of recent issue) for price information. For an electronic copy visit the MSA web site at http://www.minsocam.org, go to the American Mineralogist Contents, find the table of contents for the specific volume/issue wanted, and then click on the deposit link there.

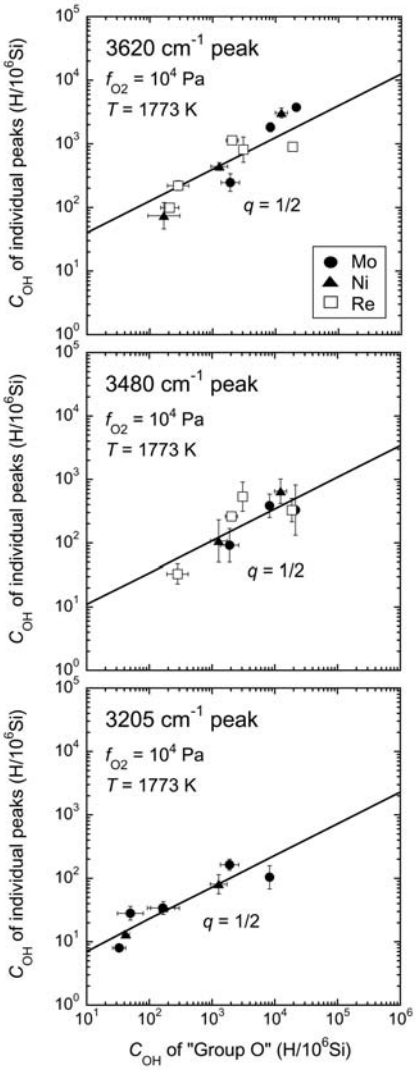

FIGURE 8. OH concentrations corresponding to peaks at 3620, 3480, and 3205 cm^{-1} plotted as a function of OH concentration of Group O ($C_{OH,Group\ O}$). Data are normalized to $f_{O_2} = 10^4$ Pa and $T = 1773$ K using parameters derived by the fit with fixed $q = 1/2$ and $r = 1/12$ or $-1/12$ (Table 2). Same symbols as Figure 2 are used for each capsule material. Fits of Equation 5 are shown as solid lines.

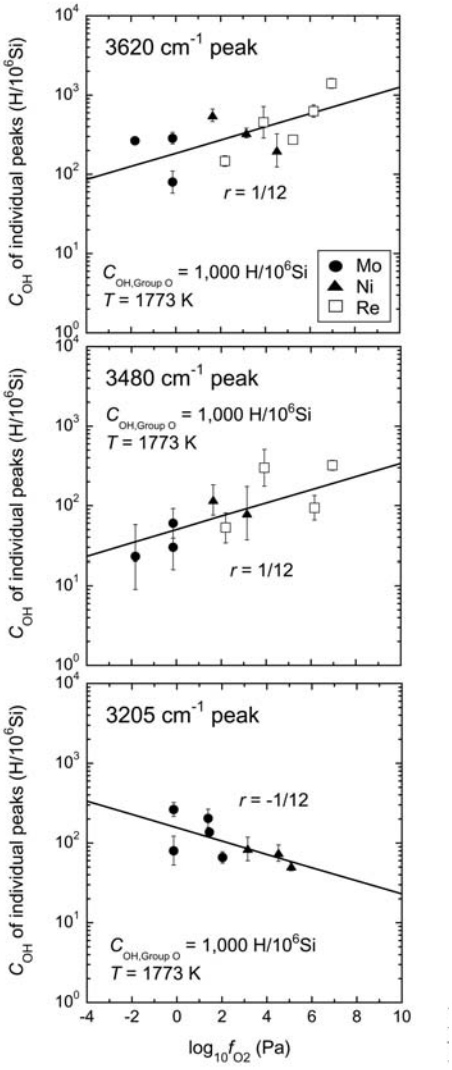

FIGURE 9. OH concentrations corresponding to peaks at 3620, 3480, and 3205 cm^{-1} plotted as a function of oxygen fugacity. Data are normalized to $C_{OH,Group\ O} = 1000$ H/10^6Si and $T = 1773$ K using parameters derived by the fit with fixed $q = 1/2$ and $r = 1/12$ or $-1/12$ (Table 2). Same symbols as Figures 2 and 8 are used for each capsule material. Fits of Equation 5 are shown as solid lines.

TABLE 4. Exponents for concentration of hydrogen-related point defects in $(Mg,Fe)_2SiO_4$ minerals

Charge neutrality condition	A			F			K		
	$[Fe_M^\bullet] = [H_M']$			$[Fe_M^\bullet] = 2[V_M'']$			$[Fe_M^\bullet] = [Fe_{Si}']$		
Defect	*q*	*r*	*s*	*q*	*r*	*s*	*q*	*r*	*s*
$[H^\bullet]$	3/4	−1/8	−1/2	1/2	−1/12	−1/3	1/2	0	3/2
$[H_M']$	1/4	1/8	−1/2	1/2	1/12	−2/3	1/2	0	−5/2
$[H_{Si}'''']$	−1/4	3/8	7/2	1/2	1/4	3	1/2	0	−5/2
$[(2H)_i^{\bullet\bullet}]$	1/2	1/4	3	1	1/6	8/3	1	0	−1
$[(3H)_{Si}']$	5/4	1/8	5/2	3/2	1/12	7/3	3/2	0	1/2
$[(OH)_O^\bullet]$	3/4	−1/8	−1/2	1/2	−1/12	−1/3	1/2	0	3/2
$[(OH)_i']$	1/4	1/8	1/2	1/2	1/12	1/3	1/2	0	−3/2

Notes: Table shows dependence of concentrations of point defects in $(Mg,Fe)_2SiO_4$ minerals on chemical environment: $[X] \propto f_{H_2O}^r f_{O_2}^r a_{MO}^s$. The name of each charge neutrality condition (e.g., A, F) is defined in Table A2.

material (Table S1)[1]. In Table S1, we also present data of the exponents of concentration of defects under other possible charge neutrality conditions. Table A2 lists all the tested combinations of defects as charge neutrality conditions.

Among three candidates described above (A, F, and K), F is the only charge neutrality condition that is consistent with the experimental constraints. Under charge neutrality condition K, concentration of all the hydrogen-related defects is independent

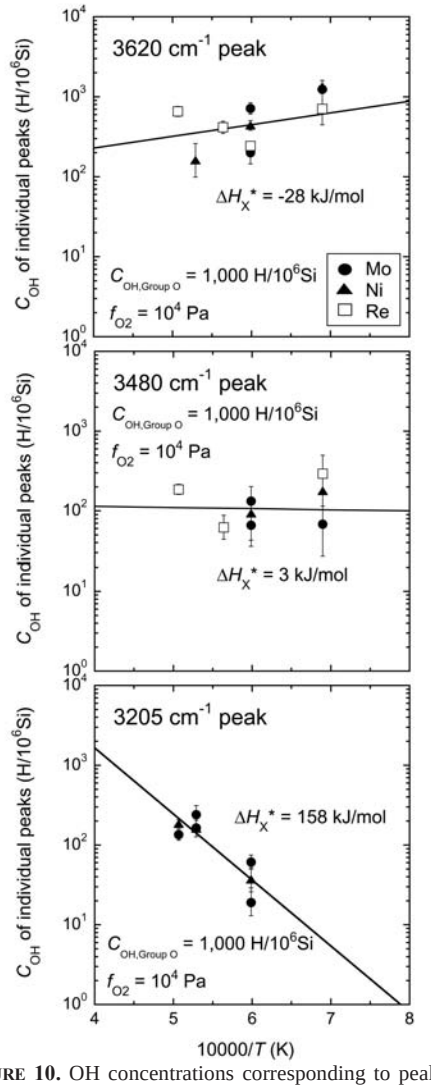

FIGURE 10. OH concentrations corresponding to peaks at 3620, 3480, and 3205 cm^{-1} plotted as a function of reciprocal temperature. Data are normalized to $C_{OH,Group\ O}$ = 1000 H/10^6Si and f_{O_2} = 10^4 Pa using parameters derived by the fit with fixed q = 1/2 and r = 1/12 or –1/12 (Table 2). Same symbols as Figures 2, 8, and 9 are used for each capsule material. Fits of Equation 5 are shown as solid lines.

of f_{O_2}, which is inconsistent with significant effect of capsule material as was observed in present experiments. In the case of charge neutrality condition A, $Fe^{\bullet}_M$ and H'_M are the most abundant charged defects. Thus "3620," which is the most dominant peak among three marked FTIR peaks, must correspond to H'_M. However, theoretical values of q = 1/4 and r = 1/8 for H'_M (Table 4) are inconsistent with experimental constraint (Fig. 7) under the charge neutrality condition A. Under charge neutrality condition F, q = 1/2 and r = 1/12 for both H'_M and $(OH)'_i$ are fairly consistent with both "3620" and "3480," and q = 1/2 and r = –1/12 for $H^{\bullet}$ [=$(OH)^{\bullet}_O$] are consistent with "3205." Therefore our observations are best explained by an effective charge neutrality condition of $[Fe^{\bullet}_M] = 2[V''_M]$ where "3620" and "3480" are corresponding to H'_M and/or $(OH)'_i$ and "3205" is corresponding to $H^{\bullet}$ [= $(OH)^{\bullet}_O$]. Among H'_M and $(OH)'_i$, H'_M is considered to be more abundant because concentration of M-site related defects, V''_M and $(2H)^x_M$], are found to be very high. Thus both of "3620" and "3480" are likely to be associated with H'_M. Note that $H^{\bullet}$ is a just simplified notation of $(OH)^{\bullet}_O$, and they refer to an identical defect.

Compatibility of the above model with present data can be visually confirmed by Figures 8 and 9. In these figures, Equation 5 is fitted with q = 1/2 and r = 1/12 for "3620" and "3480," and with q = 1/2 and r = –1/12 for "3205". We offer the parameters derived by this fit as representative results, and they are also presented in Table 2.

From the analyses of present data, only the values of ΔH^*_X could be calculated (Table 2) but values of ΔH_X could not be calculated. To discuss the formation enthalpy of defect X (ΔH_X) associated with "3620," "3480," and "3205," the data of the formation enthalpy of $(2H)^x_M$ ($\Delta H_{(2H)^x_M}$) is needed. The value of $\Delta H_{(2H)^x_M}$ was derived from a thermodynamic analysis using the chemical compositions of coexisting hydrous wadsleyite and hydrous melt at P = 15 GPa and T = 1373–1673 K reported by Demouchy et al. (2005). The analysis of the data of Demouchy et al. (2005) data are described in Appendix 2. The derived formation enthalpy of $(2H)^x_M$ is $\Delta H_{(2H)^x_M}$ = 77 kJ/mol. Using this value of $\Delta H_{(2H)^x_M}$, formation enthalpies of defect X (ΔH_X) associated with "3620," "3480," and "3205" were calculated to be $\Delta H_X = \Delta H^*_x + q\Delta H_{(2H)^x_M}$ = 11 ± 20, 42 ± 19, and 197 ± 34 kJ/mol, respectively. The ΔH_X for "3620" and "3480" were indistinguishable within the uncertainties again and were close to zero. The ΔH_X for "3205" was significantly larger than those for "3620" and "3480."

Although actual chemical reactions that yield defects H'_M and $H^{\bullet}$ could not be identified uniquely, we can offer some possible candidates. For H'_M,

$$MSiO_3 + \tfrac{1}{2}H_2O + \tfrac{1}{4}O_2 + M^x_M + Fe^x_M \leftrightarrow H'_M + Fe^{\bullet}_M + M_2SiO_4$$

or

$$\tfrac{1}{2}MSiO_3 + \tfrac{1}{2}H_2O + \tfrac{1}{2}M^x_M + \tfrac{1}{2}V''_M \leftrightarrow H'_M + \tfrac{1}{2}M_2SiO_4,$$

and for $H^{\bullet}$,

$$\tfrac{1}{2}MSiO_3 + \tfrac{1}{2}H_2O + \tfrac{1}{2}M^x_M \leftrightarrow H^{\bullet} + \tfrac{1}{2}V''_M + \tfrac{1}{2}M_2SiO_4$$

or

$$\tfrac{1}{2}H_2O + Fe^{\bullet}_M \leftrightarrow H^{\bullet} + Fe^x_M + \tfrac{1}{4}O_2.$$

The determined formation enthalpies (ΔH_X) are considered to be associated with ones of the above reactions.

In olivine, it is known that the charge neutrality condition changes from $[Fe^{\bullet}_M] = 2[V''_M]$ (F) to $[Fe^{\bullet}_M] = [H'_M]$ (A) with increasing f_{H_2O} (e.g., Karato 1989; Mei and Kohlstedt 2000). Although we did not find any evidence of the change in charge neutrality condition within the scatter of present data (see Figs. 8, 9, and 10), this might occur in wadsleyite. In the data analysis, we used Equation 5 for fitting to C_{OH} for individual peaks. This scheme is applicable only when all analyzed data are from samples with the identical charge neutrality condition. If charge neutrality condition is changed in the studied experimental conditions, the parameters (A, q, r, and ΔH^*_x) also change. Thus the fitting must be carried out individually for data at each charge neutrality condition. Further systematic studies on electrical conductivity and ionic diffusion might improve the understanding of the charge neutrality condition in wadsleyite.

Huang et al. (2005) determined water content exponents for electrical conductivity of wadsleyite and ringwoodite to be 0.66 ± 0.05 and 0.69 ± 0.03, respectively, based on the measurements of iron-bearing aggregates at their stability conditions. With assumption of charge neutrality condition of $[Fe^{\bullet}_{M}] = [H'_{M}]$ (A), they concluded that the charge carrying species both in wadsleyite and ringwoodite is $H^{\bullet}$ whose concentration is proportional to $f^{3/4}_{H_2O}$. The assumed charge neutrality condition (A) in Huang et al. (2005) is different from that proposed for wadsleyite in this study (F). However, during Huang et al.'s experiments, the water content slightly changed (~30% or less) and actual water contents during measurements are not constrained with high precision. This might yield additional uncertainty for determination of the water content exponent for electrical conductivity of wadsleyite. Thus we propose that the charge carrying species in wadsleyite is $H^{\bullet}$ under the charge neutrality condition of $[Fe^{\bullet}_{M}] = 2[V''_{M}]$ (F), whose concentration is proportional to $f^{1/2}_{H_2O}$ (Table 4). Alternatively, the observed $q = 0.66 \pm 0.05$, may reflect the fact that the charge neutrality condition changes from $[Fe^{\bullet}_{M}] = 2[V''_{M}]$ to $[Fe^{\bullet}_{M}] = [H'_{M}]$ as f_{H_2O} increases (in such a case q changes from 1/2 to 3/4).

Jacobsen et al. (2005) studied the nature of OH in three single-crystal Mg_2SiO_4 wadsleyites for a range of $C_{OH,Total}$ = 2300–150 000 H/10^6Si using polarized FTIR spectroscopy. They showed that the intensity of many FTIR peaks in wadsleyite is highly dependent on crystallographic orientation, and they determined the direction of the corresponding OH vibration. They concluded that the "3620" (a peak at 3614 or 3619 cm^{-1} in Jacobsen et al. 2005) corresponds to an absorber lying in the **a**-**c** plane. Judging from their FTIR spectra in sample WZ304 (Fig. 3b in Jacobsen et al. 2005), "3480" and "3205" correspond to an OH vibration along the **a**-**c** plane and **a**-direction, respectively. Therefore, from comparison with present results, we conclude that the OH vibration corresponding to H'_M ("3620" and "3480") is along the **a**-**c** plane and that corresponding to $H^{\bullet}$ ("3205") is along the **a**-direction.

Finally we note that the characteristic time for diffusional exchange of a defect from one site to another is so small {less than micro second above T ~1300 K [estimated from the diffusion coefficients (Hae et al. 2006) and the distance of atomic sites]} that it is unlikely that the distribution of defects at specific sites at high temperature (and pressure) can be quenched when temperature is reduced at the end of an experiment (Karato 2006). This means that even though there must be equilibrium defect concentration at a given temperature and pressure during a high *P*-*T* experiment, the concentrations of defects at various atomic sites (or the concentrations of defects with different speciation) may change differently during quenching. Consequently, the formation enthalpies that we estimated may not correspond to true formation enthalpies but may reflect the kinetics of rearrangement of defects during cooling. However, the results of the dependence of defect concentrations on the chemical environment (i.e., the exponents q and r) are robust because, during cooling, the f_{O_2} and f_{H_2O} will change with temperature similarly for various chemical environments. We therefore believe that the conclusion on the defects corresponding to each peak is robust although the significance of the estimated formation enthalpies is subject to some complications.

ACKNOWLEDGMENTS

This research is supported by the National Science Foundation. We acknowledge Zhenting Jiang, Yousheng Xu, and Kyoko N. Matsukage for technical help. We also thank Hiroyuki Kagi and his colleagues for help in FTIR analyses presented in Appendix 1, and Paras Bhalla for reading the manuscript. Paul Asimow, Jed Mosenfelder, and an anonymous reviewer provided thoughtful comments, which improved the manuscript. This work was partially supported by the Grant-in-Aid for Scientific Research to Y.N. (17740348) from Ministry of Education Culture, Sports Science, and Technology, Japan.

REFERENCES CITED

Aoki, I. and Takahashi, E. (2004) Density of MORB eclogite in the upper mantle. Physics of the Earth and Planetary Interiors, 143–144, 129–143.

Blum, J. and Shen, Y. (2004) Thermal, hydrous, and mechanical states of the mantle transition zone beneath southern Africa. Earth Planetary Science Letters, 217, 367–378.

Demouchy, S., Deloule, E., Frost, D.J., and Keppler, H. (2005) Pressure and temperature-dependence of water solubility in Fe-free wadsleyite. American Mineralogist, 90, 1084–1091.

Frost, D.J. and Wood, B.J. (1997) Experimental measurements of the properties of H_2O-CO_2 mixtures at high pressures and temperatures. Geochimica et Cosmochimica Acta, 61, 3301–3309.

Hae, R., Ohtani, E., Kubo, T., Koyama, T., and Utada, H. (2006) Hydrogen diffusivity in wadsleyite and water distribution in the mantle transition zone. Earth Planetary Science Letters, 243, 141–148.

Horiuchi, H., Akaogi, M., and Sawamoto, H. (1982) Crystal structure studies on spinel-related phases, spinelloids: Implications to olivine-spinel phase transformation and systemtics. In S. Akimoto and M.H. Manghnani, Eds., High-pressure research in geophysics, p. 391–403. CAPJ, Tokyo.

Huang, X., Xu, Y., and Karato, S. (2005) Water content in the transition zone from electrical conductivity of wadsleyite and ringwoodite. Nature, 434, 746–749.

Ichiki, M., Baba, K., Obayashi, M., and Utada, H. (2006) Water content and geotherm in the upper mantle above the stagnant slab: Interpretation of electrical conductivity and seismic P-wave velocity. Physics of the Earth and Planetary Interiors, 155, 1–15.

Inoue, T., Yurimoto, H., and Kudoh, Y. (1995) Hydrous modified spinel, $Mg_{1.75}SiH_{0.5}O_4$: A new water reservoir in the mantle transition region. Geophysical Research Letters, 22, 117–120.

Jacobsen, S.D., Demouchy, S., Frost, D.J., Ballaran, T.B., and Kung, J. (2005) A systematic study of OH in hydrous wadsleyite from polarized FTIR spectroscopy and single-crystal X-ray diffraction: Oxygen sites for hydrogen storage in Earth's interior. American Mineralogist, 90, 61–70.

Karato, S. (1989) Defects and plastic deformation in olivine. In S. Karato and M. Toriumi, Eds., Rheology of solids and of the Earth, p. 176–208. Oxford University Press, U.K.

——— (2006) Influence of hydrogen-related defects on electrical conductivity and plastic deformation of mantle minerals: A critical review. In S.D. Jacobsen and S. van der Lee, Eds., Earth's deep water cycle, p. 113–129. American Geophysical Union, Washington D.C.

——— (2008) Deformation of Earth materials: An Introduction to the rheology of the solid Earth, Chapter 10. Cambridge University Press, U.K.

Koch, M., Woodland, A.B., and Angel, R.J. (2004) Stability of spinelloid phases in the system Mg_2SiO_4-Fe_2SiO_4-Fe_3O_4 at 1100 °C and up to 10.5 GPa. Physics of the Earth and Planetary Interiors, 143–144, 171–183.

Kohlstedt, D.L., Keppler, H., and Rubie, D.C. (1996) Solubility of water in the α, β, and γ phases of $(Mg,Fe)_2SiO_4$. Contributions to Mineralogy and Petrology, 123, 345–357.

Kohn, S.C., Brooker, R.A., Frost, D.J., Slesinger, A.E., and Wood, B.J. (2002) Ordering of hydroxyl defects in hydrous wadsleyite (β-Mg_2SiO_4). American Mineralogist, 87, 293–301.

Kröger, F.A. and Vink, H.J. (1956) Relations between the concentrations of imperfections in crystalline solids. Solid State Physics, 3, 307–435.

Kubo, T., Shimojuku, A., and Ohtani, E. (2004) Mg-Fe interdiffusion rates in wadsleyite and the diffusivity jump at the 410-km discontinuity. Physics and Chemistry of Minerals, 31, 456–464.

Kudoh, Y. and Inoue, T. (1999) Mg-vacant structural modules and dilution of the symmetry of hydrous wadsleyite, β-$Mg_{2-x}SiH_{2x}O_4$ with $0.00 \le x \le 0.25$. Physics and Chemistry of Minerals, 26, 382–388.

Libowitzky, E. and Rossman, G.R. (1996) Principles of quantitative absorbance measurements in anisotropic crystals. Physics and Chemistry of Minerals, 23, 319–327.

McCammon, C.A., Frost, D.J., Smyth, J.R., Laustsen, H.M.S., Kawamoto, T., Ross, N.L., and van Aken, P.A. (2004) Oxidation state iron in hydrous mantle phases: implications for subduction and mantle oxygen fugacity. Physics of the Earth and Planetary Interiors, 143−144, 157–169.

Mei, S. and Kohlstedt, D.L. (2000) Influence of water on plastic deformation of olivine aggregates 1. Diffusion creep regime. Journal of Geophysical Research, 105, 21457−21469.

Nishihara, Y., Shinmei, T., and Karato, S. (2006a) Grain-growth kinetics in wadsleyite: Effects of chemical environment. Physics of the Earth and Planetary Interiors,

154, 30–43.
Nishihara, Y., Matsukage, K.N., and Karato, S. (2006b) Effects of metal protection coils on the thermocouple EMF in multi-anvil high-pressure experiments. American Mineralogist, 91, 111–114.
O'Neill, H.St.C. (1986) Mo-MoO_2 (MOM) oxygen buffer and the free energy of formation of MoO_2. American Mineralogist, 71, 1007–1010.
O'Neill, H.St.C. and Pownceby, M.I. (1993) Thermodynamic data from redox reactions at high temperatures. I. An experimental and theoretical assessment of the electrical method using stabilized zirconia electrolytes, with revised values for the Fe- "FeO," Co-CoO, Ni-NiO, and Cu-Cu_2O oxygen buffers, and new data for the W-WO_2 buffer. Contributions to Mineralogy and Petrology, 114, 296–314.
Paterson, M.S. (1982) The determination of hydroxyl by infrared absorption in quartz, silicate glasses and similar materials. Bulletin de Mineralogie, 105, 20–29.
Pitzer, K.S. and Sterner, S.M. (1994) Equation of state valid continuously from zero to extreme pressures for H_2O and CO_2. Journal of Chemical Physics, 101, 3111–3116.
Pownceby, M.I. and O'Neill, H.St.C. (1994) Thermodynamic data from redox reactions at high temperatures. IV. Calibration of the Re-ReO_2 oxygen buffer from EMF and NiO + Ni-Pd redox sensor measurements. Contributions to Mineralogy and Petrology, 118, 130–137.
Richet, P., Hovis, G., and Whittington, A. (2006) Water and magmas: Thermal effects of exsolution. Earth and Planetary Science Letters, 241, 972–977.
Robie, R.A., Hemingway, B.S., and Fisher, J.R. (1978) Thermodynamic properties of minerals and related substances at 298.15 K and 1 bar (10^5 pascals) pressure and at higher temperatures. U.S. Geological Survey Bulletin 1452, U.S. Government Printing Office, Washington, D.C.
Rubie, D.C., Karato, S., Yan, H., and O'Neill, H.St.C. (1993) Low differential stress and controlled chemical environment in multianvil high-pressure experiments. Physics and Chemistry of Minerals, 20, 315–322.
Smyth, J.R. (1987) β-Mg_2SiO_4: A potential host for water in the mantle? American Mineralogist, 72, 1051–1055.
Stocker, R.L. and Smyth, D.M. (1978) Effect of enstatite activity and oxygen partial pressure on the point-defect chemistry of olivine. Physics of the Earth and Planetary Interiors, 16, 145–156.
Yamanaka, T., Tobe, H., Shimazu, T., Nakatsuka, A., Dobuchi, Y., Ohtaka, O., Nagai, T., and Ito, E. (1998) Phase relations and physical properties of Fe_2SiO_4-Fe_3O_4 solid solution under pressures up to 12 GPa. In M.H. Manghnani and T. Yagi, Eds., Properties of Earth and Planetary Materials at High Pressure and Temperature, 101, p. 451–459. Geophysical Monograph, American Geophysical Union, Washington D.C.

MANUSCRIPT RECEIVED MARCH 26, 2007
MANUSCRIPT ACCEPTED DECEMBER 18, 2007
MANUSCRIPT HANDLED BY PAUL ASIMOW

APPENDIX 1

Relationship between absorbance and thickness in non-polarized FTIR analyses

Libowitzky and Rossman (1996) discussed the principles of quantitative FTIR absorbance measurements in anisotropic materials. They concluded that, when the sample is anisotropic, measurements with a non-polarized IR beam yields a non-linear relationship between absorbance and sample thickness and this makes it impossible to measure concentration of the absorber quantitatively. However, in the present study, polycrystalline aggregate wadsleyites were analyzed with non-polarized FTIR because the grain-size of the samples is generally less than 10 μm and single-crystal measurement is extremely difficult. Thus, we examined the validity of our FTIR analyses from the relationship between absorbance and thickness for wadsleyite aggregate.

The sample was synthesized from San Carlos olivine within a Re foil capsule by heating at P = 15 GPa and T = 1473 K for 1 h. For this synthesis experiment, we used a SPI-1000 Kawai-type multi-anvil apparatus installed at Magma factory, Tokyo Institute of Technology, together with the 14M/8 cell assembly (Aoki and Takahashi 2004). Average grain-size of the synthesized wadsleyite was 3.0 μm. FTIR analyses were carried out at Geochemical Laboratory, University of Tokyo using a FTIR spectrometer, Perkins Elmer, Spectrum 2000 with mid-IR light, a KBr beam splitter and MCT detector. A non-polarized IR beam with dimension of 50 × 50 μm was used. For the FTIR measurements, samples were doubly polished to thickness of 26–255 μm, which is comparable to thickness of samples analyzed and discussed in the main text (50–200 μm). Samples were directly put on a single-crystal diamond disk. The IR spectra were obtained for more than 200 scans with 4 cm^{-1} resolution. Background corrections of absorbance spectra were performed by a spline fit of the baseline. The concentration of OH was calculated to be $C_{OH,Total}$ = 7900 H/10^6Si and $C_{OH,3620}$ = 1100 H/10^6Si based on Paterson's (1982) calibration.

Figure A1 shows the FTIR absorbance spectra of the sample. The spectra show the most intense peak at 3330 cm^{-1} and weaker peaks at 3470, 3580, and 3620 cm^{-1}. The exact peak positions of these spectra are at 3327, 3474, 3581, and 3617 cm^{-1}. When the spectra were compared with other samples annealed within the Re capsule (Fig. 5), the shape of the spectra are intermediate to those of Figures 5a and 5b. This is reasonable because total water content of this sample (7900 H/10^6Si) is intermediate to those of K22 (20 000 H/10^6Si, Fig. 5a) and K23 (4900 H/10^6Si, Fig. 5b).

Figure A2 shows the relationship between absorbance at the three most intense peaks (3327, 3581, and 3617 cm^{-1}) as a function of sample thickness. It is clearly recognized from Figure A2 that absorbance is a linear function of sample thickness. The FTIR measurements on single-crystal wadsleyite by Jacobsen et al. (2005) demonstrated that peaks at 3581 and 3617 cm^{-1} are highly anisotropic and suggested that these peaks correspond to absorbers lying in the **b**-**c** and **a**-**c** planes, respectively. Figure A2 shows that, in the present case, non-linearity of absorbance-thickness relationship is not very significant even for these anisotropic peaks. Thus, we conclude that, in the studied range of sample thickness, FTIR measurement with a non-polarized beam for the polycrystalline aggregate of wadsleyite dose not yield significant errors in quantitative measurements of OH concentration.

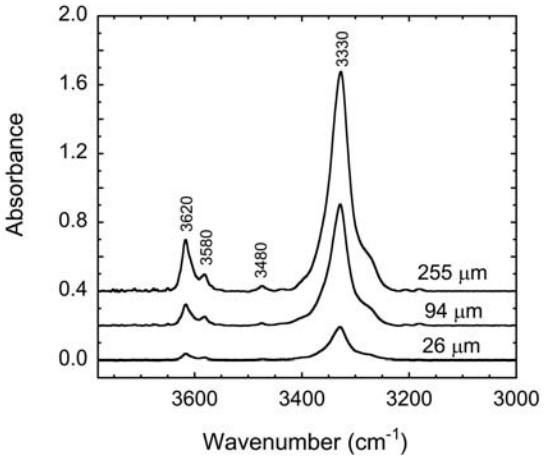

FIGURE A1. FTIR absorbance spectra of wadsleyite sample (S1516) with different thicknesses(255, 94, and 26 μm from top to bottom). The sample was synthesized from San Carlos olivine powder within a Re foil capsule by heating at P = 15 GPa and T = 1473 K for 1 h.

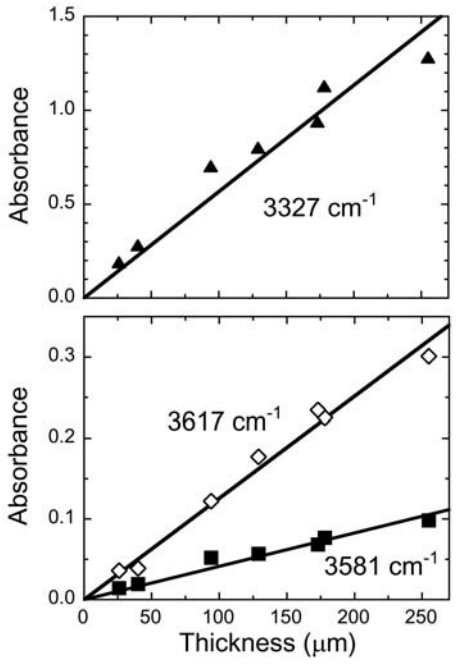

FIGURE A2. Relationship between FTIR absorbance and thickness of wadsleyite sample (S1516). Solid triangles, solid squares and open diamonds are absorbances at 3327, 3581, and 3617 cm^{-1}, respectively. The linear relationship between absorbance and thickness is clearly recognized for all three FTIR peaks.

APPENDIX 2

Determination of $\Delta H_{(2H)^x_M}$

In the present analyses, the formation enthalpy of $(2H)^x_M$ ($\Delta H_{(2H)^x_M}$) must be known to determine the formation enthalpy of the hydrogen-related defect X (ΔH_X). Since the majority of hydrogen in wadsleyite at water-rich condition is known to be $(2H)^x_M$ (e.g., Smyth 1987; Inoue et al. 1995), $\Delta H_{(2H)^x_M}$ can be determined from the temperature dependence of the water content in coexisting wadsleyite and fluid (melt). Here we will estimate the $\Delta H_{(2H)^x_M}$ of wadsleyite from the thermodynamic analysis of the data reported by Demouchy et al. (2005). Demouchy et al. (2005) determined the chemical compositions of coexisting hydrous wadsleyite and an aqueous fluid (melt) at P = 15 GPa and T = 1373–1673 K in the system MgO-SiO_2-H_2O based on phase equilibrium experiments and chemical analyses. They performed thermodynamic analysis and calculated the enthalpy change associated with hydrogen incorporation reaction in wadsleyite. However, their enthalpy change is not directly applicable as $\Delta H_{(2H)^x_M}$ due to the following two reasons: (1) the hydrogen incorporation reaction was not defined to yield $(2H)^x_M$, and (2) the temperature effects on f_{H_2O} are not treated explicitly. Therefore we reanalyzed Demouchy et al.'s (2005) data and determined $\Delta H_{(2H)^x_M}$ as follows.

Based on previous studies of wadsleyite, a maximum of 1/8 of the total Mg (and Fe^{2+}) can be replaced by 2H at relatively water-rich conditions. Thus, dry and hydrous end-members of wadsleyite solid solution are $Mg_8Si_4O_{16}$ and $Mg_7H_2Si_4O_{16}$, respectively. The hydrogen incorporation reaction based on this mechanism is

$$MgSiO_3(CEn) + H_2O(Fl) + Mg^x_M \leftrightarrow (2H)^x_M + \tfrac{1}{4}Mg_8Si_4O_{16}(Wd) \quad (A1)$$

where (CEn), (Fl) and (Wd) denote components in clinoenstatite, aqueous fluid (melt) and wadsleyite phases, respectively. $\Delta H_{(2H)^x_M}$ is defined as an enthalpy change for the reaction A1. The defect notations can be replaced by usual chemical formulae as $Mg^x_M \rightarrow Mg_8Si_4O_{16}$ and $(2H)^x_M \rightarrow Mg_7H_2Si_4O_{16}$. Thus, modification of reaction A1 can be expressed without defect notation as,

$$MgSiO_3(CEn) + H_2O(Fl) + \tfrac{3}{4}Mg_8Si_4O_{16}(Wd) \leftrightarrow Mg_7H_2Si_4O_{16}(Wd). \quad (A2)$$

The equilibrium constant K for this reaction is described as

$$K = \frac{a^{Wd}_{Hy}}{a^{CEn}_{MgSiO_3} \cdot f_{H_2O} \cdot \left(a^{Wd}_{Dry}\right)^{3/4}} \quad (A3)$$

where Dry and Hy describe two wadsleyite end-members $Mg_8Si_4O_{16}$ and $Mg_7H_2Si_4O_{16}$, respectively, a is the activity of $MgSiO_3$ in clinoenstatite, dry or hydrous end-members in wadsleyite. Since, in all the experiments used in thermodynamic analysis, $MgSiO_3$ clinopyroxene with a very small amount of impurity coexists with wadsleyite and fluid, $a^{CEn}_{MgSiO3} = 1$. Assuming an ideal solution for wadsleyite, $a^{Wd}_{Dry} = X^{Wd}_{Dry}$ and $a^{Wd}_{Hy} = X^{Wd}_{Hy}$, where X is the content of each end-member in wadsleyite. Thus Equation A3 is reduced to

$$K = \frac{X^{Wd}_{Hy}}{f_{H_2O} \cdot \left(X^{Wd}_{Dry}\right)^{3/4}}. \quad (A4)$$

The K is also expressed as

$$K = \exp\left(-\frac{\Delta G_{(A1)}}{RT}\right) = \exp\left(\frac{\Delta S_{(A1)}}{R} - \frac{\Delta H_{(A1)}}{RT}\right) \quad (A5)$$

where $\Delta G_{(A1)}$, $\Delta S_{(A1)}$, and $\Delta H_{(A1)}$ are the changes in Gibbs free energy, entropy and enthalpy for the reaction A1 (or A2), and $\Delta H_{(A1)}$ is equal to $\Delta H_{(2H)^x_M}$ as described above.

The $\Delta H_{(2H)^x_M}$ at P = 15 GPa was calculated from the temperature dependence of K using Equations A4 and A5. For the calculation, the f_{H_2O} was calculated assuming ideal solution behavior for the hydrous fluid (melt), $f_{H_2O} = X^{Fl}_{H_2O} \cdot f^{\circ}_{H_2O}$, where

TABLE A1. Chemical composition of coexisting wadsleyite and melt, water fugacity and equilibrium constant at P = 15 GPa re-calculated based on Demouchy et al.'s (2005) experimental data

T (K)	X^{Wd}_{Dry}	X^{Wd}_{Hy}	$X^{Fl}_{H_2O}$	$\log_{10} f^{\circ}_{H_2O}$ (Pa)	$\log_{10} f_{H_2O}$ (Pa)	$\log_{10} K$ (Pa^{-1})
1373	0.261	0.739	0.473	16.43	16.11	–15.80
1473	0.320	0.680	0.453	16.09	15.75	–15.54
1573	0.492	0.508	0.334	15.79	15.32	–15.38
1673	0.709	0.291	0.210	15.53	14.85	–15.28

Notes: X^{Wd}_{Dry} and X^{Wd}_{Hy} are contents of dry and hydrous end-members ($Mg_8Si_4O_{16}$ and $Mg_7H_2Si_4O_{16}$) in wadsleyite, respectively. $X^{Fl}_{H_2O}$ is H_2O content in fluid (melt) phase that is calculated as mole fraction of H_2O to total of MgO, $Si_{1/2}O$ and H_2O. $f^{\circ}_{H_2O}$ is H_2O fugacity for pure H_2O at relevant condition that is calculated from equation of state of H_2O by Frost and Wood (1997).

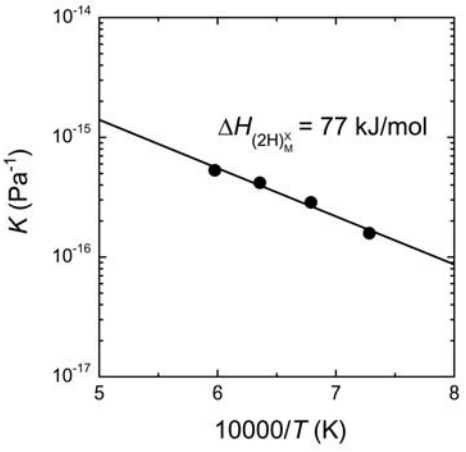

FIGURE A3. The equilibrium constant, *K*, for reaction A2 as a function of reciprocal temperature. Data are based on reanalysis of Demouchy et al.'s (2005) experimental data; see text for more detail. A least squares fit of Equation A5 to the data yielded $\Delta H_{(2H)_M^x}$ = 77 kJ/mol.

$f^{\circ}_{H_2O}$ is the water fugacity for pure H_2O fluid at relevant conditions (Frost and Wood 1997) and $X^{Fl}_{H_2O}$ is mole fraction of H_2O to total of MgO, $Si_{1/2}O$, and H_2O in aqueous fluid (melt). The input data and calculated *K* are summarized in Table A1, and a plot of *K* against reciprocal temperature is shown in Figure A3. A least squares fit of Equation A5 to *K* yielded $\Delta H_{(2H)_M^x}$ = 77 kJ/mol. When $f^{\circ}_{H_2O}$ is calculated based on the study of Pitzer and Sterner (1994), the fit yields a very similar value $\Delta H_{(2H)_M^x}$ = 80 kJ/mol. Although the mixing properties of silicate-rich aqueous fluid at high pressure is not well known, the enthalpy of mixing of H_2O and aluminosilicate melt is nearly zero at low pressure (P < 0.3 GPa) (e.g., Richet et al. 2006). If we assume non-ideal parameter of the mixing $W^{Fl}_{H_2O}$ is 0 ± 10 kJ/mol, the fit yields $\Delta H_{(2H)_M^x}$ = 77 ± 13 kJ/mol.

TABLE A2. Tested combinations of defects as a charge neutrality condition in $(Mg,Fe)_2SiO_4$ minerals

Negatively charged defect	Positively charged defect				
	$Fe_M^{\bullet}$	$H^{\bullet}$	$(3H)_M^{\bullet}$	$Si_M^{\bullet\bullet}$	$h^{\bullet}$
H_M'	A	**B**	**C**	**D**	E
V_M''	F	**G**	**H**	**I**	J
Fe_{Si}'	**K**	L	M	N	**O**
H_{Si}'''	P	**Q**	**R**	**S**	T
$(2H)_{Si}''$	U	**V**	**W**	**X**	Y
$(3H)_{Si}'$	Z	**AA**	**AB**	**AC**	AD
e′	AE	AF	AG	AH	AI

Notes: Each character denotes a charge neutrality condition (e.g. "A" and "G" are charge neutrality conditions of $[Fe_M^{\bullet}] = [H_M']$ and $[H^{\bullet}] = 2[V_M'']$, respectively). Bold characters denotes charge neutrality conditions which yield $r = 0$ for all the hydrogen-related defects. These charge neutrality conditions are unlikely for wadsleyite because our observations clearly show that OH concentration for some marked IR peaks depends on oxygen fugacity. Complete data of dependence of defect concentrations for all the studied charge neutrality conditions are provided as on-line supplementary material.